ELSEVIER

Earth and Planetary Science Letters 200 (2002) 345–355

EPSL

www.elsevier.com/locate/epsl

Production of selected cosmogenic radionuclides by muons 1. Fast muons

B. Heisinger [a], D. Lal [b], A.J.T. Jull [c], P. Kubik [d], S. Ivy-Ochs [d], S. Neumaier [e], K. Knie [a], V. Lazarev [a], E. Nolte [a,*]

[a] *Faculty of Physics, Technical University of Munich, D-85747 Garching, Germany*
[b] *Scripps Institution of Oceanography, UCSD, La Jolla, CA 92093, USA*
[c] *Physics and Atmospheric Sciences, University of Arizona, Tucson, AZ 85721 0081, USA*
[d] *Paul Scherrer Institute, c/o ETH-Hönggerberg, CH-8093 Zürich, Switzerland*
[e] *Physikalisch–Technische Bundesanstalt Braunschweig, D-38106 Braunschweig, Germany*

Received 23 July 2001; received in revised form 18 March 2002; accepted 1 April 2002

Abstract

To investigate muon-induced nuclear reactions leading to the production of radionuclides, targets made of C_9H_{12}, SiO_2, Al_2O_3, Al, S, $CaCO_3$, Fe, Ni, Cu, Gd, Yb and Tl were irradiated with 100 and 190 GeV muons in the NA54 experimental setup at CERN. The radionuclide concentrations were measured with accelerator mass spectrometry and γ-spectroscopy. Results are presented for the corresponding partial formation cross-sections. Several of the long-lived and short-lived radionuclides studied are also produced by fast cosmic ray muons in the atmosphere and at depths underground. Because of their importance to earth sciences investigations, calculations of the depth dependence of production rates by fast cosmic ray muons have been made.

Keywords: cosmogenic elements; radioactive isotopes; cross sections; production; rates

1. Introduction

The production of radionuclides in the atmosphere and in the lithosphere by cosmic radiation is principally due to four reaction mechanisms (cf. [1]): (i) energetic nuclear reactions of the nucleonic component, (ii) negative muon capture by the target nucleus, (iii) nuclear reactions of fast muons, (iv) nuclear reactions of neutrons originating from the above reactions and from both spontaneous fission of ^{238}U and α decays of $^{235,238}U$ and ^{232}Th [2]. In recent years, muon produced radionuclides have gained considerable importance as tracers in geologic and geomorphologic processes, when depths deeper than a few meters are investigated or when high erosion or ablation rates are present. Examples of these applications are determinations of exposure ages, erosion and ablation rates of geologic surfaces, dating of groundwater, measurements of neutron fluences in Hiroshima and Nagasaki arising from the first atomic bombs, solar and reactor neutrino experiments, and dark matter searches.

* Corresponding author. Tel.: +49-89-28-91-25-54; Fax: +49-89-28-91-42-80.
E-mail address: nolte@physik.tu-muenchen.de (E. Nolte).

0012-821X/02/$ – see front matter
PII: S0012-821X(02)00640-4

The results of our investigations on the production of radionuclides due to μ^- capture are reported in [3]. In this paper, we present the results of studies on the production of radionuclides by fast muons. Radionuclides produced by fast muons are also produced by the nucleonic component, the dominant nuclear reaction in the atmosphere down to sea level and in the first few meters of the lithosphere. However, at depths greater than a few meters, muon induced reactions are the dominant mode of production. For completeness, we mention that geologic applications based on results of the present study, e.g. surface exposure ages and erosion and ablation rate determinations are described in [4]. The results of fast muon irradiation of the pseudocumol (PC) target C_9H_{12}, which is the detector compound in the solar neutrino experiment BOREXINO, and studies of background counting rates for this experiment are reported in [5].

2. Muon irradiations

Experiments were performed with 100 and 190 GeV positive muon beams at the NA54 experimental setup at CERN (Fig. 1). The muon fluxes were measured using a hodoscope consisting of a scintillation counter and an ionization chamber. About 3 m of concrete blocks were used in front of the targets to generate muon showers. The energy loss of the muons in the concrete blocks was calculated to be 1.9 and 2.3 GeV [6], respectively. Assuming a shower length of 3 hg/cm^2 [7] results in mean muon energies of 98.5 and 188.2 GeV, respectively, for the shower production at the location of the targets. The lateral extent of the showers was measured with a laterally movable scintillator and with Fe, Ni and Cu monitor disks. The radioactivities of the Fe, Ni and Cu monitor disks were measured off-line by γ-spectroscopy. The lateral activation profiles of $^{56-58}$Co in Ni disks and of ^{54}Mn in Fe disks are shown in Fig. 2. The profiles can be fitted by a single Gaussian function for the central part, which is caused mainly by the primary muon beam, and by two exponential functions at larger lateral distances. These beam profiles are used to calculate the shower fluxes seen by the target disks. The targets irradiated with the fast muon beams were C_9H_{12} (pseudocumol PC), SiO_2, Al_2O_3, Al, S, $CaCO_3$, Fe, Ni, Cu, Gd_2O_3, Yb_2O_3 and Tl.

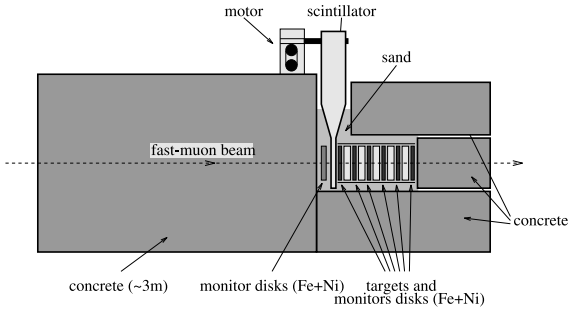

Fig. 1. Setup of experiment NA54 for irradiations of targets with fast muons.

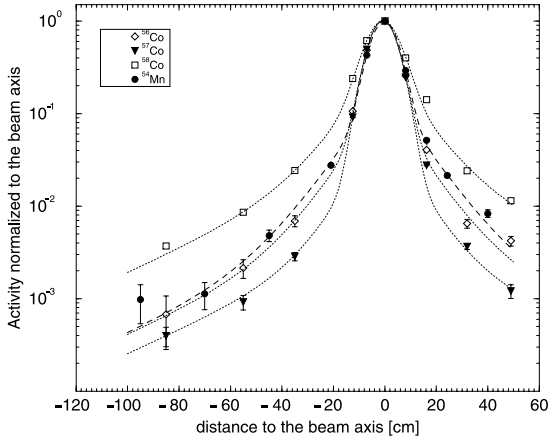

Fig. 2. Lateral activation profiles of ^{56,57,58}Co in Ni disks and of ^{54}Mn in Fe disks.

3. Chemical procedures and radionuclide measurements

For all targets except for C_9H_{12} the yields for the short-lived radioactivities were measured without chemical processing by off-line γ-spectroscopy with a shielded low-level Ge detector. The yields for the radionuclides produced from the C_9H_{12} target were measured on-line by using the target as scintillation detector (see [5]). For the concen-

tration measurements of long-lived radionuclides with accelerator mass spectrometry (AMS), the targets were chemically processed according to established procedures. Separate SiO_2 targets were used for the ^{10}Be, ^{26}Al and ^{14}C productions. The wet extraction of ^{14}C from the targets was done at the Scripps Institution of Oceanography, La Jolla, and the AMS measurements of ^{14}C were performed at the University of Arizona NSF Facility in Tucson. No chemical processing was needed for the ^{26}Al measurement in the Al_2O_3 target. The ^{10}Be targets were chemically processed as described in [8], and the $^{10}Be/Be$ ratios were determined using the AMS facility at ETH Hönggerberg [9]. All other AMS measurements were performed at the Munich accelerator laboratory. The $CaCO_3$ target was processed as described in [10] to obtain an AgCl sample. The ^{36}Cl AMS measurement was performed with completely stripped chlorine ions (see [11]). The ^{53}Mn targets were processed as described in [12] and measured using the gas-filled magnet at the Munich accelerator laboratory [12].

4. Results

The calculated cross-sections in Table 1 for muon energies of 100 and 190 GeV are based on the measured muon fluences and beam profiles, and on the nuclide concentrations measured with AMS and γ-spectroscopy. They are in the range of 2 μb–36 mb. The cross-sections for radionuclide production from the pseudocumol C target [5] are given here for completeness. ^{205}Tl from the Tl target has not yet been measured.

In the following, we discuss the implications of the results in reference to fluxes of cosmic ray muons and the expected rates of production of several nuclides.

5. Production of radionuclides by fast muons

5.1. Cosmic ray muon flux

The vertical cosmic-ray muon flux, $\Phi_v(h)$, in the lithosphere can be approximated well by [13–17]:

$$\Phi_v(h) = \frac{258.5}{(h+210)\cdot([h+10]^{1.66}+75)} e^{-5.5\times10^{-4}\cdot h} \text{ cm}^{-2}\text{ s}^{-1}\text{ sr}^{-1}$$

$$\text{for } h<2000 \text{ hg/cm}^2 \quad (1)$$

and

$$\Phi_v(h) = \left(1.82\times10^{-6}\left(\frac{1211}{h}\right)^2 e^{-\frac{h}{1211}} + 2.84\times10^{-13}\right) \text{ cm}^{-2}\text{ s}^{-1}\text{ sr}^{-1} \text{ for } h>2000 \text{ hg/cm}^2 \quad (2)$$

The lithospheric depth h is given in units of hg/cm^2 with 1 hg/cm^2 = 1 mwe (meter water equivalent). The lithospheric depth h is related to the depth z below the top of the atmosphere by $z = h+10.33$ hg/cm^2. The parametrization is identical to the one given by [13] after replacing z with the lithospheric depth h, except that the original exponent 1.68 was changed to 1.66 to obtain a smoother transition between Eqs. 1 and 2. Fig. 3 shows the vertical muon flux $\Phi_v(h)$ obtained from Eqs. 1 and 2 together with measured data [13,17–21]. The agreement is perfect over the full depth range. The zenith angle (θ) dependence of the muon flux is given by:

$$\Phi(h,\theta) = \Phi_v(h)\cdot\cos^{n(h)}\theta \quad (3)$$

where $n(h)$ can be approximated by the function:

$$n(h) = 3.21-0.297\cdot\ln(h+42)+1.21\times10^{-3}\,h \quad (4)$$

Fig. 4 shows experimental results for $n(h)$ [21–32] together with the approximation given by Eq. 4. At sea level, we obtain $n(0) = 2.1$. Using Eqs. 3 and 4, we obtain for the total muon flux, $\Phi(h)$:

$$\Phi(h) = \int_{2\pi}\Phi(h,\theta)\,d\Omega = \frac{2\pi}{n(h)+1}\cdot\Phi_v(h) \quad (5)$$

Table 1
Target element, radionuclide, half-life $T_{1/2}$, detection method, cross-sections at 100 and 190 GeV, and exponent α describing the energy dependence of the cross-section

Target	Nuclide	$T_{1/2}$	Method	σ(100 GeV) (mb)	σ(190 GeV) (mb)	α
C	^{6}He	0.807 s	in-beam γ	0.01015 ± 0.001	0.01602 ± 0.0016	0.71 ± 0.22 [5]
C	^{8}He+	0.119 s	in-beam γ			
	^{9}Li	0.178 s	in-beam γ		0.00212 ± 0.00035	[5]
C	^{8}Li	0.840 s	in-beam γ	0.00293 ± 0.0008	0.00402 ± 0.00146	0.50 ± 0.71 [5]
C	^{7}Be	53.3 days	in-beam γ	0.127 ± 0.013	0.230 ± 0.023	0.93 ± 0.23 [5]
C	^{11}Be	13.8 s	in-beam γ	< 0.00122	< 0.00234	[5]
C	^{8}B	0.770 s	in-beam γ	0.00416 ± 0.00081	0.00713 ± 0.00146	0.84 ± 0.45 [5]
C	^{9}C	0.129 s	in-beam γ		0.00483 ± 0.00151	[5]
C	^{10}C	19.3 s	in-beam γ	0.0774 ± 0.0049	0.1154 ± 0.0146	0.62 ± 0.22 [5]
C	^{11}C	20.4 min	in-beam γ	0.576 ± 0.045	0.905 ± 0.058	0.70 ± 0.16 [5]
O	^{7}Be	53.3 days	off-line γ		0.53 ± 0.11	
O	^{10}Be	1.6 Ma	AMS		0.094 ± 0.013	
O	^{14}C	5730 a	AMS		0.45 ± 0.25	
Al	^{22}Na	2.6 a	off-line γ		0.48 ± 0.08	
Al	^{24}Na	15 h	off-line γ		0.92 ± 0.15	
Al	^{26}Al	716 ka	AMS		3.3 ± 1.5	
Si	^{22}Na	2.6 a	off-line γ		0.21 ± 0.05	
Si	^{26}Al	716 ka	AMS		1.41 ± 0.17	
S	^{26}Al	716 ka	AMS		0.22 ± 0.06	
Ca	^{36}Cl	301 ka	AMS		1.40 ± 0.30	
Fe	^{46}Sc	83.8 days	off-line γ	0.097 ± 0.030	0.21 ± 0.07	1.20 ± 0.63
Fe	^{47}Sc	3.35 days	off-line γ	0.070 ± 0.025	0.085 ± 0.030	0.30 ± 0.63
Fe	^{48}V	16 days	off-line γ	0.17 ± 0.04	0.31 ± 0.09	0.88 ± 0.49
Fe	^{51}Cr	27.7 days	off-line γ	1.07 ± 0.22	2.12 ± 0.41	1.06 ± 0.39
Fe	^{52}Mn	5.6 days	off-line γ	0.14 ± 0.02	0.25 ± 0.03	0.86 ± 0.26
Fe	^{53}Mn	3.7 Ma	AMS		3.85 ± 1.1	
Fe	^{54}Mn	312 days	off-line γ	3.04 ± 0.30	5.51 ± 0.55	0.93 ± 0.21
Fe	^{56}Co	77.3 days	off-line γ	0.029 ± 0.012	0.13 ± 0.04	1.37 ± 0.68
Ni	^{46}Sc	83.8 days	off-line γ	0.044 ± 0.016	0.072 ± 0.025	0.77 ± 0.6
Ni	^{48}V	16 days	off-line γ	0.14 ± 0.04	0.27 ± 0.08	1.07 ± 0.55
Ni	^{51}Cr	27.7 days	off-line γ	0.68 ± 0.17	1.17 ± 0.30	0.84 ± 0.47
Ni	^{52}Mn	5.6 days	off-line γ	0.20 ± 0.04	0.34 ± 0.07	0.83 ± 0.39
Ni	^{54}Mn	312 days	off-line γ	0.83 ± 0.16	1.57 ± 0.31	1.00 ± 0.39
Ni	^{56}Co	77.3 days	off-line γ	1.94 ± 0.20	3.60 ± 0.38	0.96 ± 0.21
Ni	^{57}Co	272 days	off-line γ	20.2 ± 2.0	35.8 ± 3.6	0.89 ± 0.21
Ni	^{58}Co	70.9 days	off-line γ	6.11 ± 0.62	11.7 ± 1.2	1.01 ± 0.21
Ni	^{60}Co	5.27 a	off-line γ	1.77 ± 0.35	3.42 ± 0.70	1.03 ± 0.39
Ni	^{56}Ni	6.08 days	off-line γ	0.14 ± 0.03	0.27 ± 0.05	0.98 ± 0.39
Ni	^{57}Ni	36.0 h	off-line γ	4.76 ± 0.48	8.81 ± 0.85	0.96 ± 0.21
Cu	^{46}Sc	83.8 days	off-line γ	0.036 ± 0.012	0.072 ± 0.022	1.08 ± 0.55
Cu	^{48}V	16 days	off-line γ		0.085 ± 0.025	
Cu	^{51}Cr	27.7 days	off-line γ	0.185 ± 0.045	0.30 ± 0.09	0.75 ± 0.52
Cu	^{52}Mn	5.6 days	off-line γ	0.041 ± 0.012	0.080 ± 0.024	1.04 ± 0.39
Cu	^{54}Mn	312 days	off-line γ	0.21 ± 0.04	0.40 ± 0.08	1.00 ± 0.39
Cu	^{59}Fe	44.5 days	off-line γ	0.052 ± 0.010	0.120 ± 0.020	1.30 ± 0.39
Cu	^{56}Co	77.3 days	off-line γ	0.076 ± 0.014	0.155 ± 0.030	1.11 ± 0.39
Cu	^{57}Co	272 days	off-line γ	0.28 ± 0.04	0.53 ± 0.07	0.99 ± 0.30
Cu	^{58}Co	70.9 days	off-line γ	0.63 ± 0.10	1.12 ± 0.16	0.90 ± 0.30
Cu	^{60}Co	5.27 a	off-line γ	0.46 ± 0.09	1.20 ± 0.25	1.49 ± 0.39
Gd	^{153}Eu	15.2 days	off-line γ	0.11 ± 0.06		
Gd	^{157}Eu	15.2 h	off-line γ	0.35 ± 0.11		
Gd	^{159}Gd	18.5 h	off-line γ	9.3 ± 1.0		

Table 1 (*Continued*).

Target	Nuclide	$T_{1/2}$	Method	σ(100 GeV) (mb)	σ(190 GeV) (mb)	α
Gd	^{153}Gd	242 days	off-line γ	2.1 ± 0.3		
Gd	^{155}Tb	5.32 days	off-line γ	0.07 ± 0.03		
Gd	^{160}Tb	72.3 a	off-line γ	0.03 ± 0.01		
Yb	^{172}Er	49.3 h	off-line γ	0.36 ± 0.09		
Yb	^{165}Tm	30.1 h	off-line γ	0.6 ± 0.2		
Yb	^{167}Tm	9.25 days	off-line γ	1.4 ± 0.3		
Yb	^{168}Tm	93.1 days	off-line γ	0.56 ± 0.25		
Yb	^{166}Yb	56.7 h	off-line γ	0.6 ± 0.2		
Yb	^{169}Yb	32.0 days	off-line γ	7.5 ± 1.1		
Yb	^{175}Yb	4.19 days	off-line γ	27.7 ± 3.9		
Yb	^{171}Lu	8.24 days	off-line γ	0.15 ± 0.03		
Yb	^{172}Lu	6.7 days	off-line γ	0.11 ± 0.01		

The chemical compound was SiO_2 for the targets O and Si, and Al_2O_3 for Al.

5.2. Muon spectral distribution and energy spectra

Judge and Nash [24] derived the differential spectrum of the muon energy E_0 at sea level as function of the zenith angle θ:

$$D(E_0,\theta)=\frac{A_\pi W_{\mu,\pi}E_\pi^{-\gamma_\pi}H_\pi}{E_\pi\cos\theta+H_\pi}+\frac{A_K W_{\mu,K}E_K^{-\gamma_K}H_K}{E_K\cos\theta+H_K} \quad (6)$$

where E_π and E_K are the pion and kaon energies, respectively, $H_\pi \approx 114$ GeV, $H_K \approx 851$ GeV, $\gamma_\pi = \gamma_K = 2.7$, $A_\pi = 0.28$, $A_K = 0.0455$ and $W_{\mu,\pi}$ are the survival probabilities for muons in the atmosphere. For definitions of the functions $W_{\mu,\pi}$, $W_{\mu,K}$, E_π and E_K reference is made to [24]. $D(E_0,\theta)$ is used to calculate the mean muon energies but not the muon fluxes as function of depth. The total muon flux at sea level would become

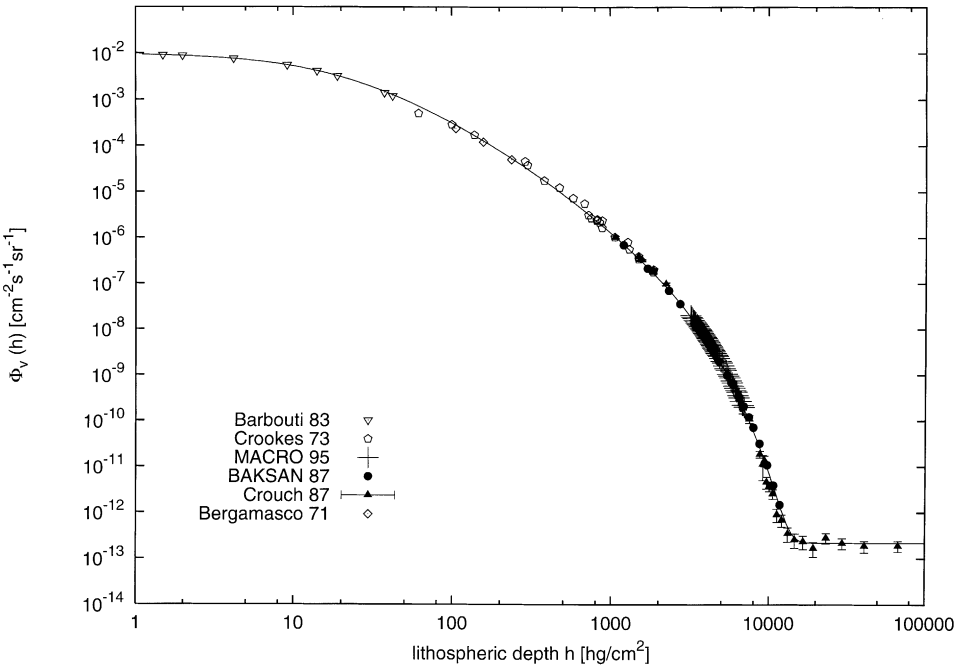

Fig. 3. Vertical cosmic ray muon fluxes $\Phi_v(h)$ calculated with Eqs. 1 and 2 in comparison with measured fluxes [13,17–21].

$\int_0^{\infty}\int_0^1 D(E_0,\theta)\mathrm{d}\cos\theta\,\mathrm{d}E_0 = 0.019\ \mathrm{cm}^{-2}\ \mathrm{s}^{-1}$. This is 10% lower than $\Phi(0) = 0.0207\ \mathrm{cm}^{-2}\ \mathrm{s}^{-1}$ from Eqs. 1, 3–5.

The energy loss of muons is given by:

$$\frac{\mathrm{d}E}{\mathrm{d}x} = a + b{\cdot}E \tag{7}$$

where a is the energy loss due to ionization and b is the sum of fractional radiation losses. The parameters a and b are almost energy independent. For standard rock and muon energies in the range around 30 GeV, $a = 0.227$ GeV hg^{-1} cm^2 and $b = 2.44\times10^{-4}$ hg^{-1} cm^2 [6].

If we consider a muon at depth h with the energy E under the angle θ, its energy $E_0(\theta,h)$ at sea level would have been:

$$E_0(\theta,h) = (E + \frac{a}{b}{\cdot})\mathrm{e}^{\frac{h\cdot b}{\cos\theta}} - \frac{a}{b} \tag{8}$$

The differential muon energy spectrum with energy E at depth h is then given by:

$$D(E,\theta,h) = D(E_0(\theta,h),\theta){\cdot}\frac{\mathrm{d}E_0(\theta,h)}{\mathrm{d}E} \tag{9}$$

with:

$$\frac{\mathrm{d}E_0(\theta,h)}{\mathrm{d}E} = \mathrm{e}^{\frac{h\cdot b}{\cos\theta}} \tag{10}$$

obtained from Eq. 8 [33].

Fluctuations in energy losses are not taken into account. With these differential energy spectra $D(E,\theta,h)$, the mean total energy $\overline{E(h)}$ and the mean vertical energy $\overline{E_\mathrm{v}(h)}$ are calculated. For sea level, $\overline{E(0)} = 7.6$ GeV and $\overline{E_\mathrm{v}(0)} = 4.6$ GeV. For shallow depths, $h < 32$ hg/cm^2, the calculated mean energies $\overline{E(h)}$ agree well with the ones given in [34]. The maximum energy at great depths, with these values of a and b, is obtained to be 350 GeV. In Fig. 5 discrete calculated mean energy values $\overline{E(h)}$ based on Eqs. 6–10 are plotted together with the experimental result of the MACRO detector [35], $\overline{E(3600\ \mathrm{mwe})} = (320 \pm 4 \pm 11)$ GeV, and with an approximation $\overline{E'(h)}$ (solid line). For the approximation $\overline{E'(h)}$, a maximum energy of 380 GeV [33] and the result of the MACRO detector were used. This approximation $\overline{E'(h)}$ (Eq. 11) facilitates the calculation of the depth dependence of the mean energy:

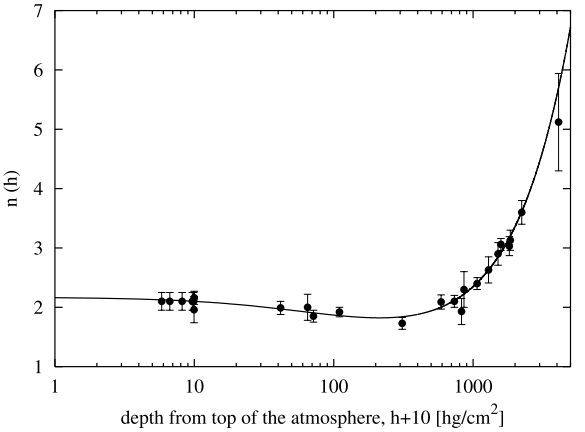

Fig. 4. Exponent $n(h)$ describing the zenith angle dependence of the muon flux via $\cos^{n(h)}\theta$ as function of the depth, h+10 hg/cm^2 below the top of the atmosphere (h is the lithospheric depth). The experimental values are taken from [21–32]. The function used for the approximation is given by: $n(h) = 3.21 - 0.297\ \ln(h+42) + 1.21\times10^{-3}h$.

$$\overline{E'(h)} = 7.6\ \mathrm{GeV} + 321.7\ \mathrm{GeV}(1-\mathrm{e}^{-8.059\times10^{-4}\cdot h}) + 50.7\ \mathrm{GeV}(1-\mathrm{e}^{-5.05\times10^{-5}\cdot h}) \tag{11}$$

5.3. Production mechanisms and production rates of nuclides by fast muons

The energy loss of muons in matter is due to ionization, direct pair production, bremsstrahlung, and inelastic nuclear scattering. The secondary particles created are δ electrons, electron/positron pairs, photons and hadrons. The electrons, positrons and photons produce electromagnetic showers, and hadronic showers are produced by hadrons and photons. The electromagnetic showers and the secondary photons produce nuclides via photo-spallation reactions. The hadronic shower particles and the secondary nucleons produce nuclides via spallation and other nuclear reactions.

The production rate of nuclides is given by:

$$P_{\mu_\mathrm{f}}(h) = \int_2\int_\pi \mathrm{d}E{\cdot}\mathrm{d}\Omega{\cdot}\Phi(h,\theta){\cdot}\sigma(E(h)){\cdot}N \tag{12}$$

where σ is the particular nuclear reaction cross-section, and N is the number of target nuclei per gram in the target compound. According to the Wolfendale rule [36–38] and based on the experimental data from the Homestake mine [39], and the Gran Sasso underground laboratory [7], the cross-section depends on the muon energy E[GeV] as:

$$\sigma(E) = \sigma_0 \cdot E^{\alpha} \tag{13}$$

with $\sigma_0 = \sigma(1\ \text{GeV})$. The exponent α is about $\alpha \approx 0.75$. For the measured nuclides σ_0 can be calculated from Eq. 13 and Table 1. With Eqs. 5, 10 and 11, the production rate of nuclides by fast muons is then given by:

$$P_{\mu_f}(h) = \sigma_0 \cdot \beta \cdot \Phi(h) \cdot \bar{E}^{\alpha}(h) \cdot N \tag{14}$$

with the factor β given by:

$$\beta(h) = \frac{\overline{E(h)^{\alpha}}}{\overline{E(h)}^{\alpha}} \tag{15}$$

Fig. 6 shows the factor $\beta(h)$ as function of the depth h for $\alpha = 0.75$. $\beta(h)$ depends only weakly on depth. For sea level, $\beta(h) = 0.85$. $\beta(h)$ can be approximated by the function:

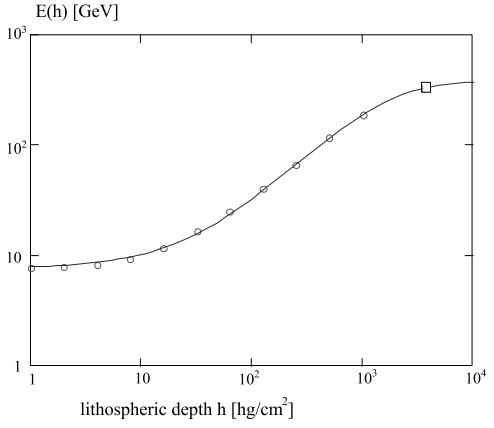

Fig. 5. Mean total muon energies $E(h)$ (○) calculated with Eqs. 6–10 as function of depth together with the approximation $E'(h)$ (solid line) of Eq. 11, and with the experimental result of the MACRO detector [17], $\overline{E(3600\ \text{mwe})} = (320 \pm 4 \pm 11)$ GeV (□).

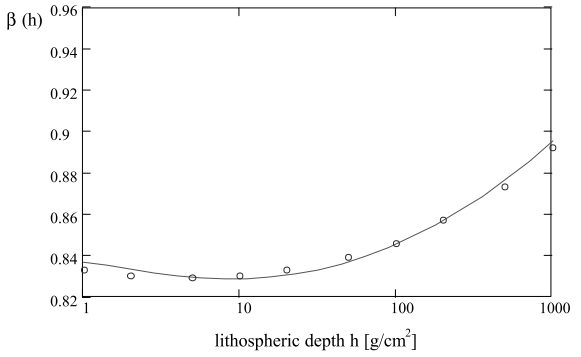

Fig. 6. Factor $\beta(h) = \frac{\overline{E(h)^{\alpha}}}{\overline{E(h)}^{\alpha}}$ as function of lithospheric depth h, calculated with Eqs. 15 and 16.

$$\beta'(h) = 0.846 - 0.015 \ln(h+1) + 0.003139\ (\ln(h+1))^2 \tag{16}$$

(solid line in Fig. 6). The mean value of β is 0.885 in [7] for greater depths, in agreement with the present calculations shown in Fig. 6.

$$\frac{P_{\mu_f}(h)}{\sigma_0 \cdot N} = \beta(h) \cdot \Phi(h) \cdot \bar{E}^{\alpha}(h) \tag{17}$$

with $\alpha = 0.75$ is shown as function of depth in Fig. 7. Using Eq. 17, it is possible to calculate the production rate of a nuclide as a function of depth if the production cross-section σ_0 is known. At sea level, we obtain:

$$\beta(0) \cdot \Phi(0) \cdot \bar{E}^{\alpha}(0) = 2.54 \times 10^6\ \text{cm}^{-2}\ \text{a}^{-1}$$

With standard mathematical programs $\beta'(h) \cdot \Phi(h) \cdot \overline{E'}^{\alpha}(h)$ can be easily calculated. Due to the calculation of the mean muon energy with Eqs. 6–10, which is different from the one used in [4,40], the present calculated yields $P_{\mu_f}(h)$ for sea level and shallow depths are higher than the ones given in [4,40]. For depths $h > 50$ hg/cm^2 relevant for fast muon induced reactions both calculated yields agree reasonably well.

The depth integrated production rate, Q_{μ_f}, of a nuclide (per cm^2 and time unit) is given by:

$$Q_{\mu_f} = \int_0^\infty P_{\mu_f}(h)\cdot dh = P_{\mu_f}(0)\cdot \Lambda_{\mu_f} \quad (18)$$

Λ_{μ_f} is the absorption mean free path for fast muon induced production of radionuclides and is calculated to be $\Lambda_{\mu_f} = 43.2$ hg/cm^2. This absorption mean free path Λ_{μ_f} can be used for rough estimates in the calculation of erosion or ablation rates, with the approximation:

$$P_{\mu_f}(h) \approx P_{\mu_f}(0)\cdot e^{-\frac{h}{\Lambda_{\mu_f}}} \quad (19)$$

The function $\beta(h)\cdot\Phi(h)\cdot\bar{E}^{\alpha}(h)$ can also be used to calculate the rate of fast muon produced neutrons. Calculated values for the energy dependent neutron production can be taken from [34,37, 38,41–43]. With [37] the depth dependent fast muon induced neutron production rate is:

$$P_{n,\mu_f}(h) = 7\times 10^{-6}\ \mathrm{g}^{-1}\ \mathrm{cm}^2\ \beta(h)\cdot\Phi(h)\cdot\bar{E}^{\alpha} \quad (20)$$

A fit to experimental results to the number N_n of produced neutrons per muon [34],

$$N_n = 4.14\cdot E_\mu^{0.74}\cdot 10^{-6}\frac{\text{neutrons}}{\text{muon}}\cdot\frac{\text{cm}^2}{\text{g}},$$

gives

$$P_{n,\mu_f}(h) = 4.8\times 10^{-6}\ \mathrm{g}^{-1}\ \mathrm{cm}^2\ \beta(h)\cdot\Phi(h)\cdot\bar{E}^{\alpha} \quad (21)$$

The yield of Eq. 21 obtained from [34] is about 70% of the yield of Eq. 20 obtained from [37].

5.4. Energy dependence of the cross-sections

In [36–38], an exponent of $\alpha = 0.75$ for the energy dependence of the cross-section is derived. Experiments for the determination of the background of neutrino experiments yield $\alpha = 0.75$ [39] and 0.7 [7], in good agreement with [36–38]. Monte Carlo simulations of the production of

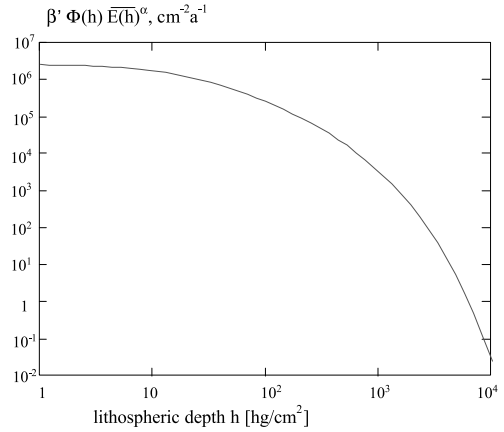

Fig. 7. Function $\beta'(h)\cdot\Phi(h)\cdot\overline{E(h)}^{\alpha}$ describing the depth dependence of the fast muon induced production rate of radionuclides, with $\alpha = 0.75$ (see text).

^{71}Ge from Gallium give $\alpha = 0.8$ [7]. The neutron yield of muons give $\alpha = 0.74$ [34]. The exponent

$$\alpha = \frac{\ln\frac{\sigma(190\ \text{GeV})}{\sigma(100\ \text{GeV})}}{\ln\frac{190}{100}}$$

deduced from the present measurements performed at 100 and 190 GeV is given in Table 1. The averaged value is $\bar{\alpha} = 0.94 \pm 0.07$. Taking energy losses in the concrete blocks in front of the targets and shower lengths into account, $\bar{\alpha} = 0.93 \pm 0.07$ is deduced. This value is slightly larger than those given in [7,34,36–39]. It is also larger than the value of $\alpha = 0.73 \pm 0.10$ [5] measured for shower production in water. This larger value can be explained by the various energy dependences of the energy loss processes of muons. The contribution of knock-on electrons from ionization losses, which is very important for energies below 100 GeV, has only a small energy dependence. Contributions of bremsstrahlung and pair production depend almost linearly on energy [44]. In water, energy loss due to ionization is more important than for concrete or standard rock. This is in agreement with the energy dependence of electromagnetic showers given by $\bar{E}^{\alpha}$ with $\alpha = 1.03 \pm 0.05$ [38]. Especially for a concrete absorber instead

of water or liquid scintillator, the last mentioned contributions are more important. This implies that for energies above 100 GeV the exponent α is significantly higher than 0.75.

σ_0 depends strongly on α. But for depths relevant for fast muon contributions with $E_\mu \geq 30$ GeV, the dependence of the production rates $P_{\mu_f}(h)$ on α is not so strong. For $E(85\ \mathrm{hg/cm^2}) =$ 35 GeV, $P_{\mu_f}(85\ \mathrm{hg/cm^2})$ calculated from $\sigma(190$ GeV) with $\alpha = 0.75$ is larger by a factor of about 1.4 than $P_{\mu_f}(85\ \mathrm{hg/cm^2})$ calculated with $\alpha = 0.94$.

Future irradiations of targets with muon energies around 30 GeV would allow to determine the cross-sections relevant for geophysical applications and α more precisely.

5.5. Examples

The measured cross-sections can be used in geological applications and for estimating background events in low-level solar neutrino experiments. Several geological applications will be described in [3]. Here the consequences for some low-level experiments are considered. Background contributions to the BOREXINO solar neutrino experiment [45] are discussed in [5]. For a proposed LiCl solar neutrino experiment [46], the ^{7}Be background due to fast muon induced reactions with the oxygen of the water solution can now be calculated. In a 12 molar LiCl aqueous solution the molar ratio LiCl to H_2O is about 1:3.5. At a depth of $h = 5000\ \mathrm{hg/cm^2}$, as e.g. for the Baksan laboratory, and for 200 tons of solution the fast muon induced production rate is two ^{7}Be nuclei/day. In the standard solar model (SSM) [47] 51.8 SNU are predicted for a ^{7}Li target (1 SNU = 10^{-36} neutrino captures/s per atom). The calculated solar neutrino induced production rate is thus 4.7 ^{7}Be nuclei/day in the 200 ton solution. Scaling this value with the ratio of the experimentally obtained 2.2 SNU for the ^{37}Cl experiment [48] to the SSM prediction of 7.9 SNU [47] results in an expected solar neutrino induced production rate of 1.3 ^{7}Be nuclei/day in the 200 ton solution of the proposed LiCl experiment. As a roughly 10% uncertainty is aspired for this experiment, the background would either have to be determined experimentally with high precision or depths greater than $h = 5000\ \mathrm{hg/cm^2}$ will have to be chosen.

6. Conclusion

In the experiments presented here, targets relevant for geological or low-level counting applications were irradiated with fast muons of 100 GeV and 190 GeV energies at CERN to obtain cross-sections for the production of several short-lived and long-lived radionuclides, which are also produced by cosmic rays in rocks. The exponent describing this energy dependence was found to be slightly greater than other reported values. This can be understood as a result of the different energy dependences for the various energy loss mechanisms.

Depth dependent production rates for fast muon produced neutrons were derived. The measured cross-sections should prove useful as a data base for various geological applications of cosmogenic nuclides, such as determinations of surface exposure ages, erosion and ablation rates, for the determination of background contributions in low-level experiments such as the solar and reactor neutrino experiments, and in searches for dark matter.

The open question remaining is the precise value of α in rock and in ice. Muon irradiations with a ratio of muon energies larger than the 1.9 of the present paper and with lower energies which are relevant for geological applications would help to clarify the situation.

Acknowledgements

This work was supported by DFG (German Research Council) and BMBF (Federal Ministry for Education and Research).*[AH]*

References

[1] B. Heisinger, M. Niedermayer, F.J. Hartmann, G. Korschinek, E. Nolte, G. Morteani, S. Neumaier, C. Petitjean, P. Kubik, A. Synal, S. Ivy-Ochs, In-situ production of

radionuclides at great depths, Nucl. Instrum. Methods B 123 (1997) 341–346.
[2] Y. Feige, B.G. Oltman, J. Kastner, Production rates of neutrons in soils due to natural radioactivity, J. Geophys. Res. 73 (1968) 3135–3142.
[3] B. Heisinger, D. Lal, A.J.T. Jull, P. Kubik, S. Ivy-Ochs, K. Knie, E. Nolte, Production of selected radionuclides by muons. 2. Capture of negative muons, Earth Planet. Sci. Lett., this issue.
[4] B. Heisinger, E. Nolte, Cosmogenic in situ production of radionuclides: exposure ages and erosion rates, Nucl. Instrum. Methods B172 (2000) 790–795.
[5] T. Hagner, R. von Hentig, B. Heisinger, L. Oberauer, S. Schönert, F. von Feilitzsch, E. Nolte, Muon-induced production of radioactive isotopes in scintillation detectors, Astropart. Phys. 14 (2000) 33–47.
[6] T.K. Gaisser, T. Stanev, Cosmic rays, Phys. Rev. D 54 (1996) 122–127.
[7] M. Cribier, B. Pichard, J. Rich, J.P. Soirat, M. Spiro, Th. Stolarczyk, C. Tao, D. Vignaud, P. Anselmann, A. Lenzing, C. Schlosser, R. Wink, J.K. Rowley, The muon induced background in the GALLEX experiment, Astropart. Phys. 6 (1997) 129–141.
[8] C.P. Kohl, K. Nishizumi, Chemical isolation of quartz for measurement of insitu-produced cosmogenic radionuclides, Geochim. Cosmochim. Acta 56 (1992) 3583–3587.
[9] H.-A. Synal, G. Bonani, M. Döbeli, R.M. Ender, P. Gartenmann, P.W. Kubik, Ch. Schnabel, M. Suter, Status report of PSI/ETH AMS facility, Nucl. Instrum. Methods B 123 (1997) 62–68.
[10] B. Dockhorn, S. Neumaier, F.J. Hartmann, C. Petitjean, H. Faestermann, G. Korschinek, H. Morinaga, E. Nolte, Determination of erosion rates with cosmic ray produced ^{36}Cl, Z. Phys. A 341 (1991) 117–119.
[11] P. Kubik, G. Korschinek, E. Nolte, Accelerator mass spectrometry with completely stripped ^{36}Cl ions at the Munich postaccelerator, Nucl. Instrum. Methods B 1 (1984) 51–59.
[12] K. Knie, T. Faestermann, G. Korschinek, AMS at the Munich gas-filled analyzing magnet system GAMS, Nucl. Instrum. Methods B 123 (1997) 128–131.
[13] A.I. Barbouti, B.C. Rastin, A study of the absolute intensity of muons at sea level and under various thicknesses of absorber, J. Phys. G 9 (1983) 1577–1595.
[14] S. Miyake, V.S. Narasimham, P.V. Ramana Murthy, Cosmic-ray intensity measurements deep underground at depth of 800–8400 m.w.e., Nuovo Cimento 32 (1964) 1505–1523.
[15] Ch. Berger et al., Experimental study of muon bundles observed in the Fréjus detector, Phys. Rev. D 40 (1989) 2163–2171.
[16] M. Aglietta et al., Neutrino-induced and atmospheric single-muon fluxes measured over five decades of intensity by LVD at Gran Sasso laboratory, Astropart. Phys. 3 (1995) 311–320.
[17] M. Ambrosio et al., Vertical muon intensity measured with MACRO at the Gran Sasso laboratory, Phys. Rev. D 52 (1995) 3793–3802.
[18] Yu. M. Andreyev, V.I. Gurentsov, I.M. Kogai, Muon intensity from the Baksan underground scintillation telescope, in: V.A. Kozyarivsky et al. (Eds.), Proc. 20th ICRC, Nauka, Moscow, 1987, pp. 200–203.
[19] M.F. Crouch, An improved world survey expression for cosmic ray vertical intensity vs. depth in standard rock, in: V.A. Kozyarivsky et al. (Eds.), Proc. 20th ICRC, Nauka, Moscow, 1987, pp. 165–168.
[20] L. Bergamasco, B. D'Ettore Piazzoli, P. Picchi, Muon intensities underground (50–4300) m.w.e. and the S.L. energy spectrum, Nuovo Cimento B 4 (1971) 59–65.
[21] J.N. Crookes, B.C. Rastin, The absolute intensity of muons at 31.6 hg cm^{-2} below sea level, Nucl. Phys. B 58 (1973) 93–109.
[22] K. Greisen, The intensities of the hard and soft components of cosmic rays as function of altitude and zenith angle, Phys. Rev. 61 (1942) 212–221.
[23] J.R. Moroney, J.K. Parry, Aust. J. Phys. 7 (1954) 423.
[24] R.J.R. Judge, W.F. Nash, Measurements of the muon flux at various zenith angles, Nuovo Cimento 35 (1965) 999–1024.
[25] D.H. Follett, J.D. Crawshaw, Cosmic ray measurements under thirty metres of clay, Proc. R. Soc. London A 155 (1936) 546–558.
[26] C.T. Stockel, A study of muons deep underground. I. Angular distribution and vertical intensity, J. Phys. A 2 (1969) 639–649.
[27] B.V. Sreekanten, S. Naranan, Proc. Indian Acad. Sci. 36 (1951) 97.
[28] L. Avan, M. Avan, C. R. Acad. Sci. 24 (1955) 1122.
[29] C.V. Achar, V.S. Narasimham, P.V. Ramama Murthy, D.R. Creed, J.B.M. Pattison, A.W. Wolfendale, The intensity and angular distribution of cosmic rays far underground, Proc. Phys. Soc. 86 (1965) 1305–1315.
[30] C.A. Randall, W.E. Hazen, The intensity and angular distribution of mu-mesons 1100 feet underground, Nuovo Cimento 8 (1958) 878–881.
[31] L.M. Bollinger, Measurements on the cosmic radiation far underground, Ph.D. thesis, Cornell University, 1951.
[32] P.H. Barrett, L.M. Bollinger, G. Cocconi, Y. Eisenberg, K. Greisen, Interpretation of cosmic-ray-measurements far underground, Rev. Mod. Phys. 24 (1952) 133–178.
[33] C. Castagnoli, A. Castellina, O. Saavedra, T.M. Kirina, R.P. Kokoulin, A.A. Petrukhin, Observation of electromagnetic interactions of high energy muons deep underground, Phys. Rev. D 52 (1995) 2673–2683.
[34] F.-F. Wang, V. Balic, G. Gratta, A. Fasso, S. Roesler, A. Ferrari, Predicting neutron production from cosmic-ray muons, Phys. Rev. D 64 (2001) 013012.
[35] M. Ambrosio et al., Measurement of the energy spectrum of underground muons at Gran Sasso with a transition radiation detector, Astropart. Phys. 10 (1999) 11–20.
[36] A.W. Wolfendale, E.C.M. Young, R. Davis, Indirect determination of the photonuclear cross section above 20 GeV, Nat. Phys. Sci. 238 (1972) 130–131.

[37] G.T. Zatsepin, O.G. Razhskaya, Calculation of neutron production by muons at different depths underground, Bull. Acad. Sci. USSR Phys. Ser. (1965) 1779–1782.
[38] R.I. Enikeev, G.T. Zatsepin, E.V. Korolkova, V.A. Kudryavtsev, A.S. Malguin, O.G. Ryazhskaya, F.F. Khalchukov, Hadrons generated by cosmic-ray muons underground, Sov. J. Nucl. Phys. 46 (1987) 883–889.
[39] E.L. Fireman, B.T. Cleveland, R. Davis, J.K. Rowley, Cosmic-ray depth studies at the homestake mine with ^{39}K and ^{37}Ar detectors, AIP Conf. Proc. 126 (1985) 22–31.
[40] B. Heisinger, Muon Induced Production of Radionuclides (in German), Dissertation, Technical University of Munich, 1998.
[41] L.B. Bezrukov, V.I. Beresnev, G.T. Zatsepin, O.G. Ryazhskaya, L.N. Stepanets, Investigation of the depth-intensity curve of nuclear events induced by cosmic-ray muons, Sov. J. Nucl. Phys. 17 (1973) 51–53.
[42] M. Aglietta et al., Neutron flux generated by cosmic-ray muons at 5200 hg/cm^2 s.r. underground depth-neutron intensity curve, Nuovo Cimento C 12 (1989) 467–477.
[43] R. Hertenberger, M. Chen, B.L. Dougherthy, Muon-induced neutron and pion production in an organic liquid scintillator at a shallow depth, Phys. Rev. C 52 (1995) 3449–3459.
[44] F.F. Kalchukov, E.V. Korolkova, V.A. Kudryavtsev, A.S. Malguin, V.G. Ryasny, O.G. Ryalzhskaya, G.T. Zatsepin, O. Saavedra, Hadrons and other secondaries generated by cosmic-ray muons underground, Nuovo Cimento 18 (1995) 517–529.
[45] L. Oberauer, Status of the BOREXINO solar neutrino experiment, Nucl. Phys. B 77 (Proc. Suppl.) (1999) 48–54.
[46] J.K. Rowley, in: G. Friedlander (Ed.), Int. Conf. on Solar Neutrinos, Brookhaven, 1978.
[47] J.N. Bahcall, R.K. Ulrich, Solar models, neutrino experiments, and helioseismology, Rev. Mod. Phys. 60 (1988) 297–372.
[48] B.T. Cleveland, T. Daily, R. Davis Jr., J.R. Distel, K. Lande, C.K. Lee, P.S. Wildenhain, J. Ullman, Measurement of the solar electron neutrino flux with the Homestake Chlorine Detector, Astrophys. J. 496 (1998) 505–526.